



This is a repository copy of *Transition States and Control of Substrate Preference in the Promiscuous Phosphatase PP1*.

White Rose Research Online URL for this paper:

<https://eprints.whiterose.ac.uk/119427/>

Version: Accepted Version

---

**Article:**

Chu, Y., Williams, N.H. [orcid.org/0000-0002-4457-4220](https://orcid.org/0000-0002-4457-4220) and Hengge, A.C. [orcid.org/0000-0002-5696-2087](https://orcid.org/0000-0002-5696-2087) (2017) Transition States and Control of Substrate Preference in the Promiscuous Phosphatase PP1. *Biochemistry*, 56 (30). pp. 3923-3933. ISSN 0006-2960

<https://doi.org/10.1021/acs.biochem.7b00441>

---

This document is the Accepted Manuscript version of a Published Work that appeared in final form in *Biochemistry*, copyright © American Chemical Society after peer review and technical editing by the publisher. To access the final edited and published work see <https://doi.org/10.1021/acs.biochem.7b00441>

**Reuse**

Items deposited in White Rose Research Online are protected by copyright, with all rights reserved unless indicated otherwise. They may be downloaded and/or printed for private study, or other acts as permitted by national copyright laws. The publisher or other rights holders may allow further reproduction and re-use of the full text version. This is indicated by the licence information on the White Rose Research Online record for the item.

**Takedown**

If you consider content in White Rose Research Online to be in breach of UK law, please notify us by emailing [eprints@whiterose.ac.uk](mailto:eprints@whiterose.ac.uk) including the URL of the record and the reason for the withdrawal request.



[eprints@whiterose.ac.uk](mailto:eprints@whiterose.ac.uk)  
<https://eprints.whiterose.ac.uk/>

**Transition States and Control of Substrate Preference in the Promiscuous Phosphatase  
PP1**

Yuan Chu,<sup>a</sup> Nicholas H. Williams\*<sup>b</sup> and Alvan C. Hengge\*<sup>a</sup>

<sup>a</sup>Department of Chemistry and Biochemistry, Utah State University, Logan, Utah 84322-0300

<sup>b</sup>Centre for Chemical Biology, Department of Chemistry, University of Sheffield, Sheffield, U.K.,  
S3 7HF

## Abstract

Catalytically promiscuous enzymes are an attractive frontier for biochemistry, because enzyme promiscuities not only plausibly explain enzyme evolution through the mechanism of gene duplication, but could also provide an efficient route to changing the catalytic function of proteins by mimicking this evolutionary process. PP1 $\alpha$  is an effectively promiscuous phosphatase for the hydrolysis of both monoanionic and dianionic phosphate-ester based substrates. In addition to its native phosphate monoester substrate, PP1 $\alpha$  catalyzes the hydrolysis of aryl methylphosphonates, fluorophosphate esters, phosphorothioate esters, and phosphodiester, with second-order rate accelerations that fall within the narrow range of  $10^{11}$  to  $10^{13}$ . In contrast to the different transition states in the uncatalyzed hydrolysis reactions of these substrates, PP1 $\alpha$  catalyzes their hydrolysis through similar transition states. PP1 $\alpha$  does not catalyze the hydrolysis of a sulfate ester, which is unexpected. The PP1 $\alpha$  active site is tolerant of variations in the geometry of bound ligands, which permit the effective catalysis even of substrates whose steric requirements may result in perturbations to the positioning of the transferring group, both in the initial enzyme-substrate complex and in the transition state. The conservative mutation of arginine 221 to lysine results in a mutant that is a more effective catalyst toward monoanionic substrates. The surprising conversion of substrate preference lends support to the notion that mutations following gene duplication can result in an altered enzyme with different catalytic capabilities and preferences, and may provide a pathway for the evolution of new enzymes.

## Introduction

Catalytic promiscuity describes the ability of an enzyme to catalyze chemically distinct reactions. This can involve forming and cleaving different type of bonds, or using more than one mechanistic pathway for the same overall bond making and breaking process. A related concept is substrate promiscuity, in which substrates with varying structures undergo the same chemical reaction with similar transition states. In both cases, the catalytic efficiencies ( $k_{\text{cat}}/K_{\text{M}}$ ) are often significantly lower than the native reaction.

In recent years the promiscuity of enzymes has drawn considerable attention for the insights offered into enzyme evolution, and for potential applications in enzyme engineering and biocatalysis. It has been proposed that promiscuity might provide a starting point for divergent evolution after gene duplication, based upon the fact that many enzymes have remarkably broad substrate specificities.<sup>1,2</sup> Observations of catalytic promiscuity in the alkaline phosphatase (AP) superfamily identified close evolutionary relationships between AP members where the promiscuous activity of one member is the native function of another.<sup>3</sup> Promiscuity has been utilized to engineer enzymes with altered activities. These results show that single or few point mutations can substantially improve the ability of enzymes to carry out new reactions.<sup>4-10</sup>

In contrast to the growing number of examples of catalytic promiscuity, the detailed study of the origins of the promiscuity is deficient.<sup>11</sup> The illustration of effects contributing to catalytic promiscuity, such as the mechanistic basis, structures of active sites, and the identification of the critical properties of substrates, are needed for a deep understanding of promiscuity, and eventually, for predicting and utilizing protein evolution pathways.

Protein phosphatase-1 (PP1), a member of the phosphoprotein phosphatase (PPP) gene family, is a metalloenzyme that utilizes a dinuclear metal center to catalyze the hydrolysis of phosphate esters using a metal-coordinated hydroxide nucleophile. Highly conserved residues bind the metal ions within approximately 3 Å of each other in octahedral coordination with a bridging hydroxyl and bridging acetate oxygen. Other cationic residues (histidine and arginine) line the active site which lies near the enzyme surface<sup>12</sup> (**Figure 1**).

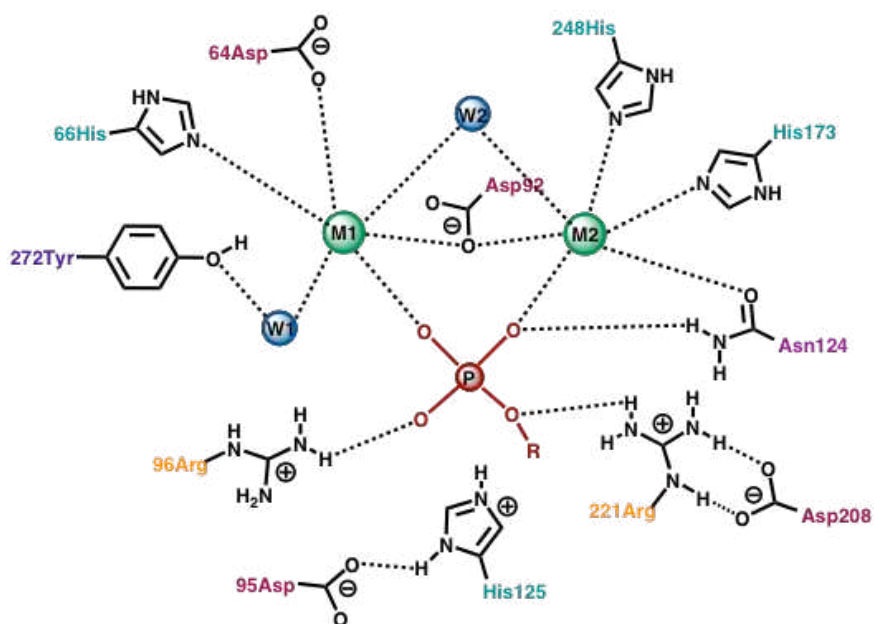


**Figure 1.** Active site of PP1 showing residues implicated in coordination of the metal ions at the active site and in substrate binding and catalysis.

Besides its native phosphate monoesterase activity PP1 exhibits activity for aryl methylphosphonate substrates.<sup>13</sup> In this work, PP1 is shown to also possess substrate promiscuity for fluorophosphate esters, phosphorothioate esters, and phosphodiester (Figure 2, structures 2, 3 and 5). These substrates vary in their intrinsic reactivity, the size and charge of the transferring group, and in the mechanisms and transition states for their uncatalyzed hydrolysis. Linear free energy relationships and kinetic isotope effects were used to probe the transition states of the PP1-catalyzed reactions compared to the uncatalyzed hydrolysis reactions.

Two active site arginine residues, R96 and R221, are implied by crystal structures to hydrogen bond to the substrate, and probably provide transition state stabilization. These were each mutated to lysine, and the effects on the respective substrate activities were assessed.

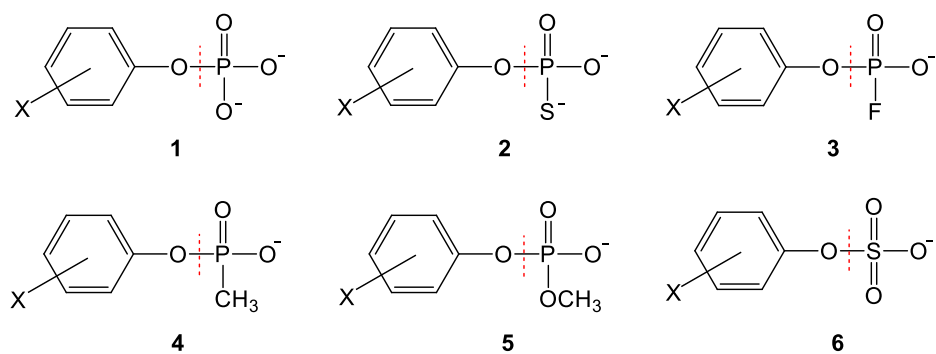


**Figure 2.** Compound classes used as substrates for PP1 catalysis. Phenyl substituents are defined in Table 1.

**Table 1.** Phenolic leaving groups used in PP1-catalyzed hydrolysis reactions with their  $pK_a$  values obtained by titration.<sup>13</sup> Data for cyano phenols are literature values.<sup>14</sup>

Phenyl substituent (X)		$pK_a$
4-NO <sub>2</sub>	a	7.01
4-Cl, 3-NO <sub>2</sub>	b	7.54
4-CN	c	7.95
3-NO <sub>2</sub>	d	8.14
3-CN	e	8.61
4-Cl	f	9.30
3-Cl	g	8.82
H-	h	9.97

## Experimental section

**General Experimental Details.** All chemical reagents and solvents were commercial products and were used as received unless otherwise noted. Thiophosphoryl chloride was distilled under nitrogen. Pyridine was distilled from calcium hydride. Acetonitrile was dried over anhydrous K<sub>2</sub>CO<sub>3</sub> for 24h followed by distillation.

**Synthesis of substrates.** 4-Nitrophenyl phosphate monoester bis(cyclohexylammonium) salt (**1a**) was prepared and purified as previously reported.<sup>15</sup> The aryl phosphorothioate bis(cyclohexylammonium) salts (**2a – h**) were prepared and purified as previously reported.<sup>16, 17</sup> The potassium salts of aryl fluorophosphate monoesters (**3a - f**) were prepared by a modification

of a literature method from 2,4-dinitrofluorobenzene and the appropriate aryl phosphoric acids in the presence of triethylamine.<sup>18, 19</sup> **3a** and **3d-f** are previously reported compounds, and NMR spectra were in agreement with those previously reported. **3b** and **3c** are new compounds. A typical procedure, described for the potassium salt of phenyl fluorophosphate monoester, was as follows. The bis(cyclohexylammonium) salt of phenyl phosphate was dissolved in a minimum amount of water. The solution was cooled, then strongly acidified with sulfuric acid and extracted with ether. The ethereal extract was combined and evaporated, leaving phenyl phosphoric acid as a thick syrup. The crude phenyl phosphoric acid (10 mmol, 1.74 g), 2,4-dinitrofluorobenzene (12 mmol, 2.23 g) and triethylamine (23 mmol, 3.2 mL) were stirred in dry acetonitrile (10 mL) at room temperature for 24 h. The solvent was evaporated, the product was dissolved in 25 mL water and treated with amberlite IR120 (H) in an ice bath and then filtered. The filtrate was washed with diethyl ether, then neutralized with potassium carbonate. The crude yellow product was obtained after lyophilization. The pure product was recrystallized from methanol/acetone/diethyl ether. 4-cyanophenyl fluorophosphate potassium salt (**3b**): <sup>1</sup>H NMR (300MHz, D<sub>2</sub>O) □/ppm 7.68 (2H, d, *J* = 6.2 Hz), 7.21 (2H, d, *J* = 8.6 Hz); <sup>31</sup>P NMR (122MHz, D<sub>2</sub>O) □/ppm -11.28 (d, *J*<sub>PF</sub> = 946 Hz); <sup>19</sup>F NMR (283MHz, D<sub>2</sub>O) □/ppm -75.41 (d, *J*<sub>PF</sub> = 946 Hz). 3-cyanophenyl fluorophosphate potassium salt (**3c**): <sup>1</sup>H NMR (300MHz, D<sub>2</sub>O) □/ppm 7.53-7.33 (4H, m); <sup>31</sup>P NMR (122MHz, D<sub>2</sub>O) □/ppm -10.76 (d, *J*<sub>PF</sub> = 946 Hz); <sup>19</sup>F NMR (283MHz, D<sub>2</sub>O) □/ppm -75.93 (d, *J*<sub>PF</sub> = 946 Hz)

*4-nitrophenyl methylphosphonate sodium salt (4a)*. The sodium salt of 4-nitrophenyl methylphosphonate was prepared according to a literature method.<sup>13</sup>

*Methyl 4-nitrophenyl phosphate diester (5a)*. The sodium salt of methyl 4-nitrophenylphosphate diester was prepared using a modification of a literature procedure.<sup>20</sup> 4-Nitrophenol (3.0 g, 21.6 mmol) in dry pyridine (10 mL) was added dropwise to a solution of phosphoryl chloride (2 mL, 21.5 mmol) in dry pyridine (25 mL). After addition was finished the mixture was stirred for another 45 min at room temperature. Methanol (1.6 mL, 40 mmol) was added slowly to the mixture, the reaction mixture then refluxed for 2 h. The reaction solution was filtered to remove pyridinium hydrochloride salt. The filtrate was added to 20 mL of cold water. The resulting solution was titrated down to pH 4-5 using HCl and extracted with dichloromethane. Removal of the solvent by rotary evaporation yielded the neutral form of

methyl 4-nitrophenyl phosphate diester. The crude product was re-dissolved in 20 mL of water and titrated to pH 9 with sodium carbonate. The pale yellow product was obtained after lyophilization. The pure product was obtained by recrystallization from acetone/methanol.  $^1\text{H}$  NMR (300MHz,  $\text{D}_2\text{O}$ )  $\delta$ /ppm 8.15 (2H, d,  $J = 8.9$  Hz), 7.23 (2H, d,  $J = 8.6$  Hz), 3.58 (3H, d,  $J_{\text{POCH}} = 11.4$  Hz);  $^{31}\text{P}$  NMR (122MHz,  $\text{D}_2\text{O}$ )  $\delta$ /ppm -3.03.

**Expression and purification of PP1 wild type.** Four isoforms of the PP1 catalytic subunit are found in mammals, and all are highly homologous and differ only in the C-terminal domain.<sup>21</sup> This work used the PP1 $\alpha$  isoform, and will be referred to as PP1 in this paper. Expression in *E. coli* DH5 $\alpha$  harboring the plasmid pCWori+ and purification were accomplished by a slight modification of the previously described method.<sup>22</sup> Briefly, the plasmid pCWori+ was used to transform competent *E. coli* DH5 $\alpha$  cells. Single colonies from *E. coli* DH5 $\alpha$  cells were taken from cells plated on LB/ampicillin plates and used to inoculate 20 mL cultures in LB/ampicillin media containing 1.0 mM  $\text{MnCl}_2$ , which were grown overnight at 37°C. These were then used to inoculate 2 liter cultures (LB/ampicillin media containing 1.0 mM  $\text{MnCl}_2$ ) and grown at 37°C until the absorbance at 600 nm reached a value of about 0.6. IPTG was then added to a concentration of 1.0 mM, and the culture was grown at room temperature for 22 hours. The bacteria were harvested by centrifugation at 8000 rpm and 4°C for 30 min. Typical yields of cell pellet were in the range 8-10 gram per liter culture. The next steps were carried out at 4°C. The resulting pellet (10 g) was resuspended in 25 mL of buffer A (0.1 mM EGTA, 25 mM triethanol amine, 1 mM  $\text{MnCl}_2$ , 0.1% v/v 2-mercaptethanol, 5% v/v glycerol, 3% by mass Brij 35, pH 7.5) containing protease inhibitors (2 mM benzamidine and 200  $\mu\text{g}/\text{mL}$  each of aprotinin, pepstatin, and leupeptin). The cells were lysed by sonication and spun down at 45,000 rpm for 30 min. The supernatant was filtered through a 0.45  $\mu\text{M}$  PES filter to remove residual debris followed by a three-step chromatographic purification that included a Heparin hi-trap column, a Q sepharose column, and a SP sepharose column. After each column, aliquots of each fraction were taken to access the progress of the purification by SDS-PAGE and pNPP activity. Enzyme-containing fractions were concentrated and stored at -80°C. Typical yield of purified PP1 was 15 mg per liter of culture. The buffer for PP1 stock solution contained 0.1 mM EGTA, 25 mM triethanol amine, 1 mM  $\text{MnCl}_2$ , 0.1% v/v 2-mercaptoethanol, 30% v/v glycerol, 3% by mass Brij 35 at pH 7.5.



**Generation of Mutants.** Primers used for each specific mutation were as follows: PP1F 5'-GGAGGTCATATGGCGGATTTAG-3'; PP1R 5'-CATCGATAAGCTTGCATGCCTGCAGCTCGAC-3'; R96K 5'-GGGGACTATGTGGACAAGGGAAAGCAG-3'; R221K 5'-GGCTGGGGTGAAAATGACAAGGAGTG. The underlined bases indicate the changes in sequence from the wild type PP1. Bases shown in bold and italic indicate the restriction sites *NdeI* (PP1F) and *HindIII* (PP1R). Site-directed mutagenesis was performed using a two-step extension overlap PCR method.<sup>23</sup> The first PCR amplification using the PP1F primer and 3' mutant primer created the DNA fragment running from the beginning of the PP1□ cDNA to the mutated sequence of interest. This procedure was also performed with the PP1R primer and 5' mutant primer to give the other section running from the beginning of the mutated sequence to the end of PP1□ cDNA. The PCR conditions used were 95°C for 1 min for 1 cycle, followed by 30 cycles consisting of 95°C for 30 seconds, 50°C for 30 seconds, 72°C for 1 minute; followed by 72°C for one 3 min cycle. The resulting PCR product was purified and applied to the second PCR amplification with the PP1F primer and PP1R primer to give the full length mutated PP1□ cDNA. The PCR conditions for the second round amplification were, for the first 5 cycles, 95°C for 30 seconds, 45°C for 40 seconds 72°C for 90 seconds; and for the remaining 35 cycles, 95°C for 30 seconds, 58°C for 30 seconds, and 72°C for 1 minute. The PCR product was purified using the Qiagen MinElute gel extraction kit and subjected to digestion with *NdeI* and *HindIII*. This fragment was ligated into the pCWOri+ vector, which was previously digested with *NdeI*/*HindIII* and purified by agarose gel electrophoresis. The construct was then used to transform competent DH5□ cells. The mutant plasmid DNA was isolated from the culture using Qiagen Miniprep DNA purification kit and sent for sequencing. The mutant of PP1 was expressed and purified as described for PP1 wild type.

**Kinetic measurements.** For the reactions producing 4-nitrophenol, reactions were followed by measuring the absorbance of the product at 400 nm in a Spectramax plate reader at 25 °C. All of the reactions were performed in buffered solutions (50 mM Tris, 50 mM Bis-Tris, 100 mM NaOAc, 0.05 mM MnCl<sub>2</sub>). Enzymatic reactions were quenched by adding 1.5 M sodium carbonate bringing the final pH to ≥ 10. The literature value of the extinction coefficient for the 4-nitrophenolate anion of 18300 cm<sup>-1</sup> M<sup>-1</sup> was used.<sup>24</sup> Initial rates (less than 5% of the

reaction) were determined at a range of substrate concentrations and used to construct Michaelis-Menten plots. Values for  $V_{\max}$  and  $K_M$  were obtained by fitting the data to the Michaelis-Menten equation using a nonlinear least-squares fit (Kaleidagraph, Synergy Software). Values of  $k_{\text{cat}}$  were obtained by dividing  $V_{\max}$  by the enzyme concentration. For reactions with other leaving groups, reactions were followed by reverse phase analytical HPLC (Agilent Eclipse XDB-C18 column,  $4.6 \times 150$  mm,  $5 \mu\text{m}$ ). The substituent phenol products were eluted using an isocratic gradient of methanol and water. The composition of the eluting solution and detection wavelength were altered for each phenol to reach the optimum separation and retention time. Table S1 in Supporting Information gives the detection wavelength and retention times for each phenol (**b** – **h** in Table 1). A concentration calibration curve for each substituent phenol was constructed using concentration ranges of 5 – 300  $\mu\text{M}$ . The concentrations of phenol product from the enzyme assay were determined by integration of the peak area at this wavelength and interpolation of the calibration curve. The literature  $\text{p}K_a$  for each substituent phenol was used in the Brønsted plot.<sup>25</sup>

**Inhibition measurements.** The rates of PP1-catalyzed *p*NPP hydrolysis in the presence of the inhibitors were determined by measuring the formation of the 4-nitrophenolate product at 400 nm as described above. Inhibitor concentrations were in the range between  $1/5$ -fold to 3-fold times  $K_i$ . The initial rates were fitted to Lineweaver–Burk plots to determine the type of inhibition. All inhibitors produced lines intersecting on the y-axis, consistent with competitive inhibition. A sample plot is provided in the Supporting Information. The resulting apparent  $k_{\text{cat}}^{\text{app}}/K_M^{\text{app}}$  values were plotted against the inhibitor concentration ( $[I]$ ) and fitted to **Equation 1** to obtain the inhibition constant ( $K_i$ ). For inhibition experiments with magnesium and aluminum fluorides, the  $\text{AlF}_x$  and  $\text{MgF}_x$  species were generated *in situ* from aluminum or magnesium chloride and sodium fluoride. Control experiments showed that neither aluminum or magnesium chloride alone, nor sodium fluoride, are inhibitory at concentrations below 50 mM. These inhibition experiments included from 2- to 6-fold excess sodium fluoride stoichiometry relative to Al or Mg. Previous inhibition experiments with other enzymes suggest that the inhibitory ion has the  $\text{MF}_3$  stoichiometry.<sup>26-28</sup>

$$\frac{k_{\text{cat}}^{\text{app}}}{K_M^{\text{app}}} = \frac{k_{\text{cat}}/K_M}{1 + \frac{[I]}{K_i}} \quad \text{Equation 1}$$

**Isotope effect measurements.** The  $^{18}\text{O}$  kinetic isotope effects with **2a** were measured by the remote label method, using the nitrogen atom in the nitro group as a reporter for isotopic fractionation in the labeled oxygen positions. **Figure 3** shows the positions at which KIEs were measured. The experimental procedures used were the same used to measure KIEs in other phosphoryl transfer reactions in which the leaving group is 4-nitrophenol<sup>29</sup> and as previously reported for **1a** and **4a**.<sup>13</sup> The details of the data analysis for the reactions of **2a** are given in the Supporting Information.

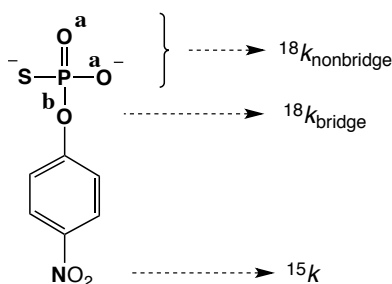


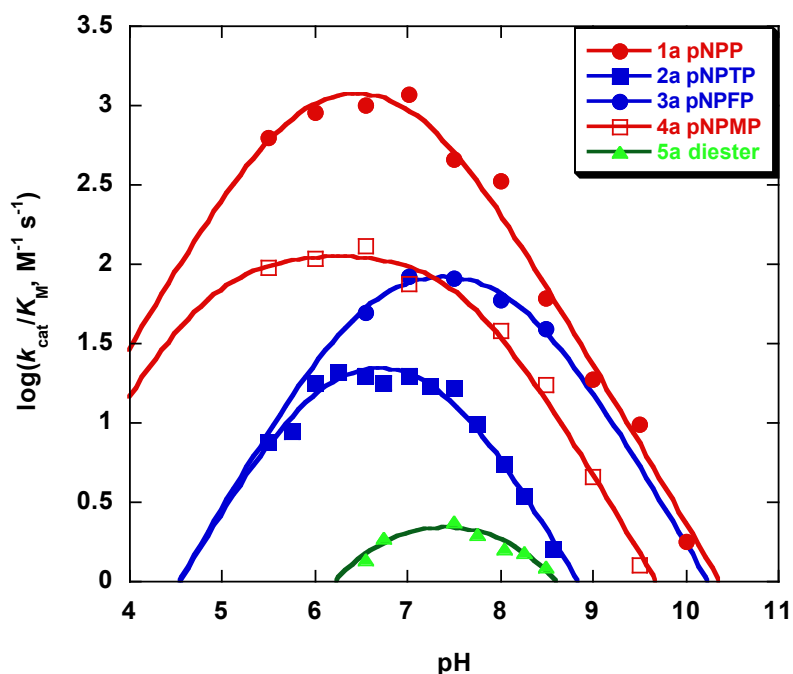
**Figure 3.** The substrate *p*NPPT (**2a**) with the positions indicated at which isotope effects were measured.

**Test for sulfatase activity.** Both control and enzymatic reactions were assayed by measuring the absorbance of the 4-nitrophenolate product at 400 nm at 25 °C. Both were performed in buffered solutions (50 mM Tris, 50 mM Bis-Tris, 100 mM NaOAc, 0.05 mM  $\text{MnCl}_2$ , 3 mM DTT, pH 7.0). The concentration of *para*-nitrophenyl sulfate potassium salt was 9.3 mM, and PP1 concentrations up to 134.6  $\mu\text{M}$  were used. A control reaction was set up identically but without PP1. After 15 hours, the changes in absorbance at 400 nm for both reactions were less than 0.003 absorbance units. The test for the PP1 R96K and R221K mutants led to the same observation. Assuming a lower limit for product detection based on a change of 0.005 absorption units,  $\sim 0.7 \mu\text{M}$  of product could have been detected under these conditions.

## Results

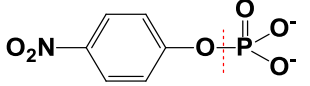
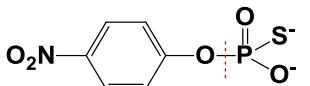
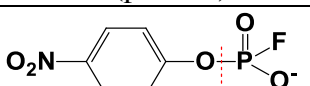
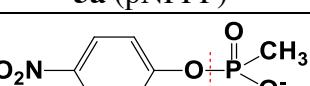
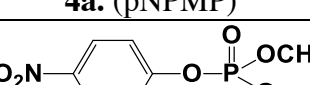
**Hydrolysis of different substrate classes by PP1 wild type.** PP1 performs multiple turnovers with each phosphate substrate examined, and saturation kinetics was observed for all substrates except *p*-nitrophenyl sulfate, **6**. No enzymatic activity with the sulfate ester was detected for either wild type PP1 or mutants. The pH dependencies of  $k_{cat}/K_M$  for substrates **2a**, **3a**, and **5a** were measured and show a bell-shaped profile indicative of catalysis by both acidic and basic residues (**Figure 4**). For the pH range sampled the protonation states of the substrates do not change. The data were fitted to **Equation 2**, derived on the assumption that the active ionic form requires one acidic (defined by  $K_a^1$ ) and one basic residue (defined by  $K_a^2$ ). The derived  $pK_a$  values and values of  $(k_{cat}/K_M)^{lim}$  are shown in first three columns in **Table 2**. The previously reported pH profiles for substrates **1a** and **4a** are also shown in **Figure 4**.

$$\frac{k_{cat}}{K_M} = \left(\frac{k_{cat}}{K_M}\right)^{lim} \left(\frac{K_a^1[H^+]}{K_a^1K_a^2 + K_a^1[H^+] + [H^+][H^+]}\right) \quad \text{Equation 2}$$



**Figure 4.** pH-rate profiles of  $k_{cat}/K_M$  for the hydrolysis of five different substrate types catalyzed by PP1: **2a** (■), **3a** (●) and **5a** (▲) are from this work; **1a** (●) and **4a** (□) have been previously reported.<sup>13</sup> Solid lines are from fits to Equation 2.

**Table 2.** The kinetic  $pK_a$  values for the wild type PP1-catalyzed hydrolysis of substrates **1a-5a** at 25 °C derived from fits to Equation 2. Substrates **2a**, **3a** and **5a** are from this work. Data for substrates **1a** and **4a** were previously reported.<sup>13</sup>

substrates	$pK_{a1}$	$pK_{a2}$	$k_{cat}/K_M^{lim}$ ( $M^{-1} s^{-1}$ )	$k_w$ ( $M^{-1} s^{-1}$ )	$(k_{cat}/K_M^{lim})/$ $k_w$
 <b>1a</b> (pNPP)	6.0±0.2	7.2±0.2	1850±500	2.3 x 10 <sup>-11</sup>	8.0 x 10 <sup>13</sup>
 <b>2a</b> (pNPTP)	6.0±0.1	7.4±0.1	31±4	1.8 x 10 <sup>-10</sup>	1.7 x 10 <sup>11</sup>
 <b>3a</b> (pNPFP)	6.5±0.1	8.2±0.1	105±15	2 x 10 <sup>-10</sup>	5 x 10 <sup>11</sup>
 <b>4a</b> . (pNPMP)	6.0±0.2	7.2±0.2	240±30	1.8 x 10 <sup>-11</sup>	1.3 x 10 <sup>13</sup>
 <b>5a</b> (pNP diester)	7.2±0.2	7.5±0.2	0.98±0.4	1.2 x 10 <sup>-13</sup>	8.2 x 10 <sup>12</sup>

**Comparisons with uncatalyzed hydrolysis and rate accelerations.** The fifth column of **Table 2** ( $k_w$ ) lists the second-order rate constants for the uncatalyzed reactions with water of substrates **1a**, **2a**, **4a**, and **5a**. These were obtained from literature information as follows. For **1a**, the pseudo-first order rate constant of 1.3 x 10<sup>-9</sup> s<sup>-1</sup> for the water reaction at 25°C was calculated from reported activation parameters<sup>30</sup> and divided by 55M to obtain the second order rate constant. Similarly, for **2a**, the pseudo first order rate constant of 9.8 x 10<sup>-9</sup> s<sup>-1</sup> at 25°C was calculated from reported activation parameters<sup>16</sup> and divided by 55M. The second order rate constant shown for **4a** has been reported previously at 30°C and 60 °C,<sup>31</sup> and the Eyring equation was used to predict the rate constant at 25 °C. For **5a**, an estimate of 1.3 x 10<sup>-11</sup> s<sup>-1</sup> was obtained for the reaction of bis-4-nitrophenyl diester with water by using the reported temperature dependence of the spontaneous hydrolysis of the bis-2,4-dinitrophenyl diester and LFER data for symmetrical diaryl phosphate diesters at 100 °C. An Eyring plot for the bis-2,4-dinitrophenyl diester hydrolysis was constructed, and the assumption made that the bis-4-nitrophenyl diester will have the same intercept (effectively assuming that the entropy of activation is the same for

the two compounds). The LFER data at 100 °C were used to generate a second point for this compound, and the two points used to estimate the rate of hydrolysis at 25 °C. This number is statistically corrected for the two leaving groups (the effect of the non-leaving group on phosphate diester hydrolysis is small, unlike the effect in phosphate triesters)<sup>32</sup> and for the concentration of water to give the value in **Table 2**. The rate constant for the water reaction of fluorophosphate ester **3a** has been measured at 80 °C ( $4 \times 10^{-7} \text{ s}^{-1}$ ), but without activation parameters (Nick Williams and Mohamed Sasi, unpublished data). However, this reaction can be compared with the second order rate constants for reaction with hydroxide at this temperature ( $0.058 \text{ M}^{-1} \text{ s}^{-1}$ ), to give a ratio of  $7 \times 10^{-6}:1$ . If the enthalpy of activation is at least as large as for the specific base catalyzed reaction, then the ratio at 25 °C will be at least as small. As the second order rate constant for reaction with hydroxide has also been measured at 42 °C, it can be estimated as  $3 \times 10^{-5} \text{ M}^{-1} \text{ s}^{-1}$  at 25 °C. Combining this with the ratio of reactivity at 80 °C leads to the estimate shown in **Table 2** as an upper limit.

The ratio of  $k_{cat}/K_M^{lim}$  to  $k_w$  gives the second order rate acceleration provided by PP1. These vary from  $1.7 \times 10^{11}$  to  $8.0 \times 10^{13}$ , which are in the range of values observed for other catalytically promiscuous enzymes, such as BcPMH.<sup>33</sup> It is noted that even with a reduction in the rate for **4a** to account for the 5°C difference in temperature, the rate acceleration for this substrate will still fall within the bounds of the other substrates.

**LFER and KIE measurements.** The leaving group dependency of the PP1-catalyzed hydrolysis reactions were used to obtain the Brønsted slope ( $\beta_{LG}$ ) for the log of  $(k_{cat}/K_M)$  versus  $\text{p}K_a$  of the leaving phenolate at pH 7.0 for the series of phosphorothioate (**2**) and fluorophosphate (**3**) esters using the aryl leaving groups in **Table 1**. The diester substrate (**5**) reacted too slowly to obtain LFER data. The results are compared with previous data from phosphate monoesters and methyl phosphonate esters. **Figure 5** shows the Brønsted plots for the substrate classes **1-4**. The slopes are collected in **Table 3** and shown with the values for the corresponding nonenzymatic hydrolysis reactions. The Brønsted slopes for all of the PP1-catalyzed reactions lie within the range -0.25 to -0.40, while those for the nonenzymatic reactions are more variable. Insufficient data exists to compare the Brønsted slopes of substrate classes 1-4 for their water and hydroxide reactions. However, data for both nucleophiles on phosphate diesters show that the  $\beta_{LG}$

decreases modestly ( $\sim 0.2$  units) for the stronger nucleophile, although exact comparison is not possible due to differences in reaction conditions and in the diesters themselves.<sup>34</sup>

**Table 4** gives the KIEs for the PP1-catalyzed reactions of substrates **1a**, **2a**, and **4a**. Syntheses for the needed double-labeled forms of **3a** could not be carried out with sufficient isotopic purity for KIE determinations. All KIEs were measured by the competitive method, in which a mixture of the isotopic isomers is present in solution. Measurement of KIEs using the competitive method yields the isotope effect on  $(V/K)$ , or, the isotope effect on the rate-limiting step for the part of the overall reaction sequence up to and including the first irreversible step. For PP1-catalyzed reactions this will be P-O bond fission, and thus, the isotope effects will reflect this chemical step even if a subsequent step such as product release is rate-limiting in the overall kinetic mechanism.

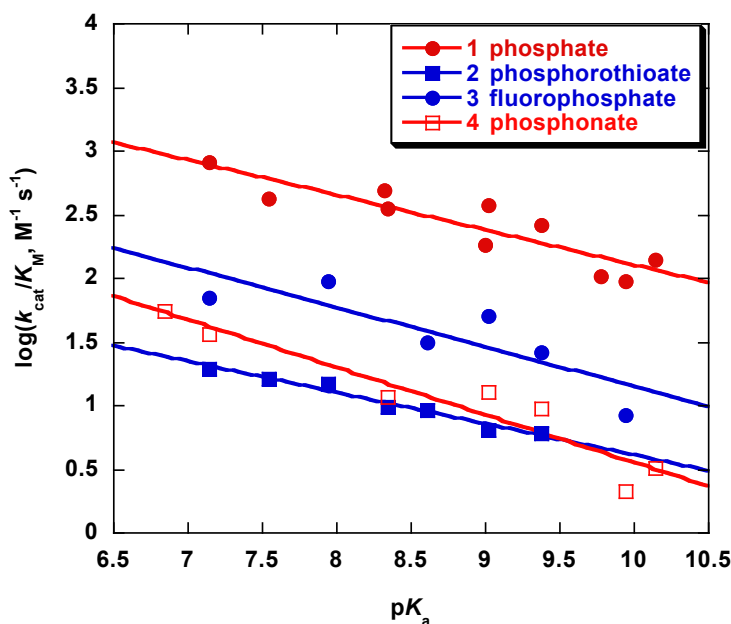


**Figure 5.** Brønsted plot for the PP1-catalyzed hydrolysis of four substrate classes: aryl phosphorothioate monoesters **2** (■) and aryl fluorophosphate monoesters **3** (●) are from this work; aryl phosphate monoester dianions **1** (●) and aryl phosphonate monoesters **4** (□) are from previous work.<sup>13</sup>

**Table 3.** Brønsted  $\beta_{LG}$  values for the PP1-catalyzed and the nonenzymatic hydrolysis reactions of substrate types **1-4** with either water or hydroxide.

Substrate class	$\beta_{LG}$ for PP1-catalyzed reaction	$\beta_{LG}$ for nonenzymatic hydrolysis
<b>1</b>	-0.32 <sup>13</sup>	-1.23 <sup>24</sup> (water)
<b>2</b>	-0.25 ± 0.02	-1.1 <sup>35</sup> (water)
<b>3</b>	-0.40 ± 0.07	-0.63 <sup>36</sup> (hydroxide)
<b>4</b>	-0.30 <sup>13</sup>	-0.69 <sup>13</sup> (hydroxide)

**Table 4.** KIE data for uncatalyzed and PP1-catalyzed reactions. New data from this study for substrate **2a** are in bold.

	Results for 2a ( <i>p</i> NPTP)		Results for 1a ( <i>p</i> NPP)		Results for 4a ( <i>p</i> NPMP)	
	Dianion H <sub>2</sub> O attack, 50°C <sup>35, 37</sup>	PP1-catalyzed	Dianion H <sub>2</sub> O attack, 95°C <sup>24, 38</sup>	PP1-catalyzed <sup>13</sup>	Monoanion OH attack, 25°C <sup>13</sup>	PP1-catalyzed <sup>13</sup>
<sup>18</sup> <i>k</i> <sub>nonbridge</sub>	1.0135 (13)	<b>0.9717 (18)</b>	0.9994 (5)	0.9959 (4)	1.0015 (4)	0.9973 (4)
<sup>18</sup> <i>k</i> <sub>bridge</sub>	1.0237 (7)	<b>1.0161 (5)</b>	1.0189 (5)	1.0170 (3)	1.0098 (4)	1.0129 (3)
<sup>15</sup> <i>k</i>	1.0027 (1)	<b>1.0001 (1)</b>	1.0028 (2)	1.0010 (2)	1.0006 (3)	1.0010 (1)

**Inhibition.** Table 5 reports the inhibition constants for the species that were tested as inhibitors of PP1 as described in the Experimental Section. Competitive inhibition was found in all cases. For the metal fluoride species, fits of the data to **Equation 1** assumed that the concentration of inhibitory species equaled the concentration of Mg or Al. Since not all of the metal will be in the correct inhibitory complex state with fluoride, these fits give an underestimation of the inhibition constants of the putative MF<sub>3</sub> species. Magnesium chloride and sodium fluoride alone were very weak inhibitors, with estimated inhibition constants of ~70 mM (MgCl<sub>2</sub>) and ~150 mM (NaF).



**Table 5.** Inhibition of the PP1-catalyzed hydrolysis of **1a** (pNPP) by inhibitors at pH 7.0. Inhibition constants for  $\text{MgF}_x$  and  $\text{AlF}_x$  were calculated as described in the Experimental section.

Inhibitor	Geometry	$K_i$ (mM)	Inhibitor	Geometry	$K_i$ (mM)
	Tetrahedral	$1.2 \pm 0.2$		Tetrahedral	$36 \pm 2$
	Tetrahedral	$3.0 \pm 0.2$		Tetrahedral	$22 \pm 2$
$\text{PF}_6^-$	Octahedral	$5.6 \pm 0.8$		Tetrahedral	$30 \pm 2$
$\text{BF}_4^-$	Tetrahedral	$8 \pm 2$			
$\text{MgF}_x$	planar	$0.83 \pm 0.06$		Tetrahedral	$40 \pm 9$
$\text{AlF}_x$	planar	$0.032 \pm 0.003$			

**Hydrolysis of substrates 1a-5a by PP1 mutants.** The R221K and R96K mutants and the double mutant were tested for the hydrolysis of the nitrophenyl substrates **1a-5a**. Reduced rates of some mutants did not permit a full pH-rate profile to be obtained, so catalysis of each mutant compared with native PP1 at pH 7.0, shown in Table 6. The R96K mutant was less active than R221K mutant for all substrate classes. The R221K mutant was found to be a more efficient enzyme for the hydrolysis of the monoanionic substrates **3a** and **4a** than wild type PP1.

**Table 6.** Catalytic efficiencies ( $k_{\text{cat}}/K_{\text{M}}$ ,  $\text{M}^{-1}\text{s}^{-1}$ ) for the hydrolysis of substrates **1a-5a** at pH 7.0 by wild type and arginine mutants of PP1.

Substrates	WT			R96K	R221K	Double mutant
	$k_{\text{cat}}$ ( $\text{s}^{-1}$ )	$K_{\text{M}}$ (mM)	$k_{\text{cat}}/K_{\text{M}}$ , ( $\text{M}^{-1}\text{s}^{-1}$ )	$k_{\text{cat}}/K_{\text{M}}$ , ( $\text{M}^{-1}\text{s}^{-1}$ )	$k_{\text{cat}}/K_{\text{M}}$ , ( $\text{M}^{-1}\text{s}^{-1}$ )	$k_{\text{cat}}/K_{\text{M}}$ , ( $\text{M}^{-1}\text{s}^{-1}$ )
<b>1a</b>	3.2±0.1	3.6±0.3	869±3	60±8	315±31	18±2
<b>2a</b>	0.029±0.001	1.5±0.1	20±3	0.8±0.1	1.9±0.21	--- <sup>a</sup>
<b>3a</b>	0.76±0.03	9.2±0.4	83±7	25±12	157±8	17±8
<b>4a</b>	1.12±0.07	13±1	86±8	11±2	115±10	5.7±0.7
<b>5a</b>	0.016±0.001	9.2±0.9	1.7±0.3	0.35±0.08	1.8±0.4	--- <sup>a</sup>

a. the activity is too slow to be accurately measured.

## Discussion

**The transition states of the PP1-catalyzed reactions are more similar than the transition states of the uncatalyzed reactions.** The substrate classes may be grouped into two types by charge: the dianionic **1** and **2**, and the monoanionic **3-6**. PP1 efficiently catalyzes the hydrolysis of five of the six substrate classes. These esters also differ in the size of the group undergoing transfer from the ester group to water, and have pronounced differences in the mechanism and transition states of their uncatalyzed hydrolysis reactions. The uncatalyzed reactions of phosphate monoester dianions (**1**) are concerted and have a loose transition state with extensive bond fission to the leaving group and little bond formation to the nucleophile.<sup>24, 30, 37-40</sup> Phosphorothioates (**2**) react via an  $\text{S}_{\text{N}}1$  ( $\text{D}_{\text{N}}+\text{A}_{\text{N}}$ ) mechanism in which a (thio)metaphosphate intermediate is formed.<sup>16, 35, 41</sup> Sulfate monoesters (**6**) hydrolyze by loose transition states similar to those for the hydrolysis of phosphate monoester dianions.<sup>42</sup> In contrast, the reaction mechanisms of substrates **3-5** are concerted, with a tighter transition state with less bond fission to the leaving group and significant bond formation to the nucleophile.<sup>13, 20, 36, 39</sup> Of interest is whether the transition states of the PP1-catalyzed reactions retain these differences.

Linear free energy relationships (LFER) were applied to characterize transition states for the PP1-catalyzed hydrolysis of aryl phosphorothioates **2** and aryl fluorophosphate monoesters **3**.

The Brønsted coefficient  $\rho_{LG}$  is defined as the slope of rate constants versus leaving group  $pK_a$ , reflecting the extent of bond cleavage in transition states. ~~Values of  $\rho_{LG}$  for the PP1-catalyzed hydrolysis of **2** and **3** are similar to one another (Figure 5 and Table 3) and to previously reported data for substrate types **1** and **4**.~~ The  $\rho_{LG}$  values for the four substrate classes for which such data could be obtained show that their values for the enzymatic reactions fall within a much narrower range (-0.25 to -0.40) than the uncatalyzed reactions (-0.63 to -1.23). This suggests that, in contrast to the uncatalyzed reactions, the PP1-catalyzed reactions share more similar transition states. The reduced  $\rho_{LG}$  values are consistent with the proposal that H125 carries out general acid catalysis, as previously proposed based on structural data and comparisons of the active site with related metallophosphatases.<sup>12, 43</sup>

Like the  $\rho_{LG}$  values, the KIEs for the three substrate classes measured are more similar to one another than the same data for their uncatalyzed reactions. ~~To further characterize the enzymatic transition states, KIEs for PP1-catalyzed hydrolysis of **2a** were measured. KIEs for the PP1 reaction with substrates **1a** and **4a** have been previously measured.~~ Like the  $\rho_{LG}$ , the KIEs in the leaving group for PP1-catalyzed reaction of **2a** are diminished from their values in the uncatalyzed hydrolysis, as expected from general acid catalysis. The magnitude of  $^{15}(V/K)$  reflects negative charge developed on the leaving group in the transition state. For **2a**, the  $^{15}(V/K)$  of unity indicates that leaving group neutralization is complete, and is more effective than with substrates **1a** and **4a**. Why general acid catalysis should be more effective with **2a** is not clear, but the magnitude of the Brønsted  $\rho_{LG}$  slope for **2a** is also slightly smaller than the other substrate types. The leaving group  $^{18}(V/K)_{bridge}$  is affected by P-O bond fission and by protonation. With the nitrophenyl leaving group, this KIE may be as large as 1.035 when there is no inverse contribution from protonation.<sup>29</sup> The  $^{18}(V/K)_{bridge}$  in the PP1-catalyzed hydrolysis of **2a** is similar to previously obtained values for reactions of **1a** in which the transition state is characterized by extensive P-O bond fission and concurrent protonation of the leaving group.<sup>29</sup> In the uncatalyzed hydrolysis of **2a**, the magnitude for  $^{18}k_{bridge}$  implies a large degree of P-O bond fission in the transition state, and  $^{15}k$  demonstrates that the leaving group departs as the charged anion. In the PP1-catalyzed hydrolysis reaction of **2a** the magnitude of  $^{18}(V/K)_{bridge}$  is reduced, consistent with general acid protonation of the leaving group, hypothesized to be carried out by histidine 125. This KIE is also similar to those of substrates **1a** and **4a**, supporting the notion from the Brønsted  $\rho_{LG}$  data that the transition state is similar in each enzymatic reaction.

The other oxygen KIE,  $^{18}(V/K)_{\text{nonbridge}}$ , is significantly inverse, in contrast to the normal KIE for the solution hydrolysis. This same switch to an inverse  $^{18}(V/K)_{\text{nonbridge}}$  has been noted previously in the alkaline phosphatase-catalyzed reaction of **2a**, and ascribed to an inverse effect arising from coordination of the thiophosphoryl group to the metal center.<sup>17, 35</sup> Both LFER and KIE data indicate that the PP1-catalyzed hydrolysis reactions for all substrate types have similar transition states, with extensive P-O bond fission involving general acid protonation of the leaving group.

We conclude that, while the uncatalyzed hydrolysis reactions of these substrates proceed through quite different transition states, the transition states of their PP1-catalyzed reactions are more similar. Interactions between substrates and the active site are different than those with water in solution. These interactions will affect vibrational modes as well as characteristics of the transition state, and similar strong active site interactions across the substrate classes are likely responsible for the observed similarities in the LFER and KIE data for the PP1-catalyzed reactions. The notion that PP1 is able to modify transition states is consistent with recent computational analyses of factors that contribute to promiscuity, although other such enzymes, such as alkaline phosphatase, appear to accommodate variable transition states in the same active site.<sup>44</sup>

**PP1-catalyzed hydrolysis of phosphorothioate monoesters, fluorophosphate monoesters and phosphonate monoesters follow the same catalytic mechanism proposed for phosphate monoester hydrolysis.** The pH-rate profiles for the substrates (**1a – 5a**) are bell-shaped and largely coincide with a similar pH optimum, indicating the same active site and enzymatic mechanism is followed. The deduced kinetic  $pK_a$  values obtained from fits to **Equation 2** are listed in **Table 2**. Based on the crystal structure of PP1 and related Ser/Thr phosphatases, a metal-coordinated water molecule is proposed to be the nucleophile and the deprotonation of this species is likely represented by  $pK_{a1}$ .<sup>12</sup> Although the values for  $pK_{a1}$  obtained for esters **2a** and **3a** differ slightly (6.0 and 6.5, **Table 2**), plotting  $k_{\text{cat}}$  for **2a** and **3a** yields identical values for  $pK_{a1}$  ( $pK_{a1} = 6.5 \pm 0.1$ ) of the ES complex. These  $pK_a$  values are consistent with the assignment of the lower  $pK_a$  to a metal-bound water.<sup>45</sup> The fitted kinetic  $pK_{a1}$  value for substrate **5a** is about 1  $pK_a$  unit higher than the other substrate classes. The residue H125 is plausibly assigned to act as a general acid, responsible for the basic limb of the pH-rate

profile. The differences in  $pK_a$  values from the pH-rate profiles for the fluorophosphate and the methyl phosphate diester, compared to the other substrates, are greater than experimental uncertainty but are of uncertain origin. It is possible that small local differences in solvation or side chain interactions, resulting from differences in sterics, charge, and polarizability of these substrates are responsible. These are monoanionic substrates, but the differences cannot be due to charge alone, as the monoanionic methyl phosphonate exhibits values for  $pK_{a1}$  and  $pK_{a2}$  that match the natural dianionic monoester substrate.

**Binding of substrates and inhibitors is affected more by charge than size.** The values for  $K_M$  for substrates **1a-5a** at pH 7.0 are shown in **Table 6**. The dianionic substrates **1a** and **2a** have the best affinity, as expected for a phosphatase for which dianionic monoesters are the natural substrates. The lower  $K_M$  of the phosphorothioate may reflect the previously noted preference of  $Mn^{2+}$  to coordinate sulfur ligands.<sup>46, 47</sup> The higher  $K_M$  values for monoanionic substrates **3a**, **4a**, and **5a**, and the similarity of the  $K_M$  for **3a** and **5a**, indicates that loss of a negative charge has a larger effect on binding to PP1 than the addition of steric bulk by addition of a methyl or methoxyl in place of a nonbridging oxygen atom.

To further investigate the relative influences of size, geometry, and charge on affinity for the active site of PP1, a series of small molecule ionic inhibitors with various geometries were examined. The left side of the Table 5 compares the affinity of inorganic phosphate to a series of fluoride-based inhibitors. Phosphate monoesters undergo reaction by a concerted mechanism with trigonal bipyramidal transition state. Of the tested inhibitors, only the metal fluorides are able to assume this geometry. As phosphate analogues, the metallic fluorides  $AlF_x$  and  $MgF_x$  have been shown to be useful chemical probes for structural and mechanistic studies in phosphoryl transfer reaction because they are able to mimic the transition state for phosphoryl transfer when  $x = 3$ . The Al-F bond has a similar length as the P-O bond (1.5-1.6Å). It is believed that aluminofluorides can adopt tetrahedral, trigonal bipyramidal, and octahedral geometries in a protein active site.<sup>48, 49</sup> Magnesium fluoride complexes with trigonal bipyramidal and octahedral geometries have been found in active sites of proteins in X-ray structures.<sup>26, 50</sup> Here, while neither magnesium, aluminum, or fluoride ion alone are effective inhibitors, strong inhibition is observed in combination. This indicates that the inhibitory species are magnesium fluoride and aluminum fluoride complexes formed *in situ*. It is not certain what geometry these

metallic fluoride inhibitors adopt in the active site of PP1, but based on precedents with other phosphoryl transfer enzymes, a trigonal bipyramidal geometry with three fluorides in equatorial positions is most likely.  $^{19}\text{F}$  NMR has been used to successfully characterize  $\text{MgF}_3$  complexes at an enzymatic active site<sup>26</sup> but was unsuccessful here due to the presence of paramagnetic  $\text{Mn}^{2+}$  ions.

The simple fluoride salt NaF shows negligible inhibition of PP1. In contrast, fluoride has been found to significantly inhibit the activity of bovine spleen purple acid phosphatase (PAP), a member of a related class of metallophosphatases with a dinuclear metal center, with  $K_i$  ranging between 2 mM to 3  $\mu\text{M}$  depending upon the pH and metal in the active site.<sup>51</sup> Crystal structures show fluoride displaces the hydroxide bridging the two metal ions in PAP.<sup>52</sup>

Unexpectedly, the octahedral hexafluorophosphate anion is also a competitive inhibitor with  $K_i = 5.6$  mM, lower than that for tetrafluoroborate. To the best of our knowledge this is the first example of an octahedral anion inhibitor of a phosphatase.

Together, the results indicate that the binding of anions to the active site of PP1 is more affected by charge than geometry. The ability of the PP1 active site to accommodate ions of differing conformations but similar charge is consistent with its ability to catalyze reactions of differing substrates, and to modify their transition states.

#### **PP1 has high, and similar, catalytic efficiencies towards the substrate classes 1-5.**

The five substrate types (**Figure 2**) hydrolyzed by PP1 have differences in their charge, steric requirements, and in the transition states for their respective uncatalyzed hydrolysis reactions. The  $k_{\text{cat}}/K_M^{\text{lim}}$  for five substrates (**1a – 5a**) obtained from the pH profiles (**Table 2**) allows a comparison of catalytic efficiencies among substrates at optimum pH. For wild type PP1, catalytic efficiency decreases in the order **1a>4a ~ 3a>2a ~ 5a**. The difference in  $k_{\text{cat}}/K_M^{\text{lim}}$  from the fastest to the slowest substrate is only ~2000-fold. Catalytic efficiencies for the monoanionic substrates **3a** and **4a** are superior to that for **2a**, although **2a** shares the dianionic charge of phosphate monoesters that are the natural substrates for PP1.

Due to slower rates, the full pH-rate profiles needed to fit  $k_{\text{cat}}/K_M^{\text{lim}}$  for the five substrates catalyzed by the mutants were not obtainable. However,  $k_{\text{cat}}/K_M$  data at pH 7.0 was obtained for all three mutants for the five substrate types, and show the same trends as the wild type (**Table 6**).

The pH 7.0 data for substrates **1a-5a** show the same trends in catalytic efficiency as the limiting ( $k_{\text{cat}}/K_{\text{M}}^{\text{lim}}$ ). Variations in the molecular properties of the substrates affect  $k_{\text{cat}}$  more than  $K_{\text{M}}$ .

PP1 is a less efficient catalyst for the hydrolysis of phosphorothioate esters **2** than for phosphate esters **1**. Reduced catalytic effectiveness for phosphorothioates has also been reported in alkaline phosphatase<sup>17, 35, 53, 54</sup> and in protein-tyrosine phosphatases.<sup>23, 55, 56</sup> This is opposite from the effect of sulfur substitution on the uncatalyzed reaction; phosphorothioate monoesters undergo hydrolysis faster than their phosphate ester counterparts. The reduced enzymatic rates have been attributed to reduction in transition state stabilization, resulting from poorer affinity of the enzyme for the transition state of the phosphorothioate substrate. Sulfur substitution has several consequences on charge distribution and geometry; compared to oxygens in the nonbridging positions, sulfur has greater negative charge and less double bond character<sup>57, 58</sup> as well as a larger Van der Waals radius and longer bond length (1.94 Å versus 1.57Å).

In the fluorophosphate substrates, the substitution of a non-bridging oxygen by fluoride retains the size and hydrogen bond donor/acceptor properties of the phosphoryl group in the natural monoester substrate. The  $k_{\text{cat}}$  at pH 7.0 for **3a** is only ~4-fold lower than **1a**; the higher  $K_{\text{M}}$  results in an overall catalytic efficiency that is about an order of magnitude lower than **1a**. The methyl substitution (**4a**) for a nonbridging oxygen atom maintains a similar bond length around the reaction center but removes hydrogen bond donor-acceptor properties and reduces the negative charge. The  $k_{\text{cat}}$  for **4a** is only 3-fold lower than **1a** at pH 7.0, while the overall catalytic efficiency is about an order of magnitude lower. For the fluorophosphate and methylphosphonate substrates the  $k_{\text{cat}}$  and  $K_{\text{M}}$  values are similar to one another. The methoxyl substitution (**5a**) on a nonbridging oxygen atom converts the substrate into a diester, which will have the largest steric requirement of all of the substrates tested. The  $k_{\text{cat}}$  is most strongly affected by this substitution, lower by ~200-fold compared to **1a** and  $k_{\text{cat}}/K_{\text{M}}$  is more than 400-fold reduced.

The second order rate constants for the reactions of these compounds with water are all very low, reflecting the fact that these hydrolysis reactions have high kinetic barriers. This constant for the fluorophosphate ester has not been determined and is difficult to obtain due to domination by the hydroxide rate, but is probably similar to the other monoanionic substrates. The ratio of the enzymatic catalytic efficiency ( $k_{\text{cat}}/K_{\text{M}}^{\text{lim}}$ ) to the second-order rate constant for the

reaction with water ( $k_w$  in **Table 2**) gives the second-order rate enhancement, a measure of the degree to which PP1 reduces the activation barrier for the hydrolysis reactions. These values are all high and vary over a narrow range of only  $\sim 2$  orders of magnitude, and correspond to reductions in activation energy of from 16 to 19 kcal mol<sup>-1</sup>. This demonstrates that PP1 is an effective catalyst for all of these substrates despite the variations in size and charge of the transferring group. For comparison, the promiscuous *BcPMH*, assigned as a member of the alkaline phosphatase superfamily, exhibits second-order rate accelerations ranging from 10<sup>7</sup> to as high as 10<sup>19</sup> for a range of phosphate monoester, diester, and triester substrates, as well as sulfate monoesters, corresponding to decreases in the energy of activation between 14.4 and 27.2 kcal mol<sup>-1</sup>.<sup>33</sup> The hydrolase *BcPMH* uses a formyl glycine nucleophile and a single metal ion, features commonly found in sulfatases. The larger and more variable rate accelerations of *BcPMH* suggest that its active site provides the potential for additional effects that synergize with the reactivity of the metal ion. The different active site of PP1 provides a smaller, and more uniform, stabilization of catalysis toward different substrate classes.

**A simple Arg to Lys mutant of PP1 exhibits catalytic efficiency toward monoanionic substrates that are superior to wild type.** The structure of PP1 suggests that residues R96 and R221 hydrogen bond with the substrate oxygens and probably contribute to substrate binding and stabilization of the transition state. In a previous report, the R96E mutant exhibited a 700-fold lower catalytic efficiency toward the physiological substrate phosphorylated phosphorylase *a*.<sup>43</sup> A smaller effect on  $K_M$  indicates that this residue is more critical for catalysis than substrate recognition. The R96A mutant exhibited a large decrease in  $k_{cat}$  ( $>400$ -fold) but no significant change in  $K_M$ .<sup>59</sup> The R221S mutant exhibited a large reduction in  $k_{cat}$  ( $\approx 200$ -fold),<sup>59</sup> but in contrast to the R96A mutant, also showed a significant reduction in affinity for the phosphorylase *a* substrate ( $\sim 10$ -fold increase in  $K_M$ ).

The catalytic promiscuity of members of the alkaline phosphatase family has been attributed, in part, to the ability of certain side chains in the active site reposition, in order to accommodate more sterically demanding substrates.<sup>60, 61</sup> The relatively similar catalytic proficiencies for the substrate classes may result from a similar factor in PP1. Inspection of the crystal structure and hypothetical binding mode (Figure 1) suggests R96 and R221 as candidates,



as neither has a direct catalytic role but may donate a hydrogen bond. We investigated the mutations of R96 and R221 to lysine, with the hypothesis that this change would maintain hydrogen bond donating ability while providing additional space for the more sterically demanding substrates. Based on potential enzyme-substrate interactions suggested from the crystal structure, it was anticipated that the R96K mutant would be more effective in this regard. The kinetic parameters  $k_{\text{cat}}$  and  $k_{\text{cat}}/K_{\text{M}}$  were obtained for the nitrophenyl esters at pH 7 for the R96K and R221K mutants, and for the double mutant.

**Table 6** shows the catalytic efficiencies at pH 7.0 for the wild type PP1 and the arginine mutants for substrates **1a-5a**. **Table S2** shows the full set of  $k_{\text{cat}}$  and  $K_{\text{M}}$  data. Both the R96K and R221K mutations have minor effects on  $K_{\text{M}}$  and primarily affect  $k_{\text{cat}}$ , consistent with R96A and R96E results. Most interestingly, the mutant R221K exhibits  $k_{\text{cat}}$  and  $k_{\text{cat}}/K_{\text{M}}$  values superior to the native enzyme for the monoanionic substrates **3a** and **4a**. For the monoanionic diester **5a** the values are similar. This is suggestive of a more important role for R221 in stabilization of the transition state than in binding substrate. Precedent for mutations in catalytically promiscuous enzymes resulting in altered preferences for different substrates is found in the alkaline phosphatase and the related phosphate monoesterase PafA, where mutations alter the monoesterase/diesterase preferences.<sup>61, 62</sup>

***p*-Nitrophenyl sulfate is not a substrate for PP1.** The fact that *p*-nitrophenyl sulfate (pNPS) is not a substrate is surprising in light of the promiscuity of PP1 for monoanionic phosphorus-based substrates. Sulfate and phosphate monoesters share tetrahedral geometry with comparable bond angles and lengths. The uncatalyzed hydrolysis reactions of sulfate and phosphate monoesters occur with similar rate constants and with similar transition states. This similarity between phosphoryl and sulfuryl transfer reactions is reflected in the ability of several other promiscuous enzymes, including alkaline phosphatase, the sulfatase PAS, and the aforementioned *Bc*PMH that carry out both activities.<sup>63</sup> The inability of PP1 to catalyze pNPS hydrolysis is not due to an inability to bind to the active site. Inhibition experiments demonstrate that **6a** binds to the active site, albeit weakly, as a competitive inhibitor ( $K_{\text{i}} = 40$  mM). The significantly higher  $K_{\text{i}}$  compared to the monoanionic phosphoester substrates is in keeping with the weaker affinity of sulfate as a metal ligand compared with phosphate. However, even at high

substrate concentrations and long reaction times, no activity with *p*NPS was observed. The reason for this discrimination is not clear.

Inhibition experiments show that sulfate and sulfate analogues are weak competitive inhibitors of the phosphate monoesterase activity of PP1, with inhibition constants ( $K_i$ ) ranging 22 mM to 40 mM (**Table 5**). Even with the same molecular geometry, changing the center atom from phosphorus to sulfur or selenium increases the  $K_i$  by an order of magnitude.

## Conclusions

PP1 is an effective catalyst for the hydrolysis of both monoanionic and dianionic phosphate-ester based substrates **1-5**. The second-order rate accelerations are significant and similar across the range of monoanionic and dianionic substrates, ranging from  $10^{11}$  to  $10^{13}$ . The transition states for the PP1-catalyzed reactions are more similar than the transition states for the uncatalyzed hydrolysis reactions. Thus, PP1 catalyzes their hydrolysis by transition states that are controlled by the active site environment more than by the intrinsic nature of the substrates. The reason for the inability of PP1 to catalyze the hydrolysis of a sulfate ester is unclear, and unexpected, since the charge and transition state of this substrate are well within the range of those of the phosphorus-based substrates whose hydrolysis are effectively catalyzed.

Inhibition experiments suggest that the PP1 active site is tolerant of variations in the geometry of bound ligands. This characteristic may assist the effective catalysis of substrates whose steric requirements result in perturbations to the positioning of the transferring group both in the initial enzyme-substrate complex, and in the transition state.

The mutation of arginine 221 to lysine results in a mutant that, relative to the native enzyme, has reduced catalytic efficiency toward dianionic substrates but somewhat higher efficiency for the monoanionic substrates. The surprising result in substrate preference from a single, conservative mutation lends support to the notion that modest mutations can result in an enzyme with different catalytic capabilities and preferences, and may, following subsequent mutations, provide a pathway for the evolution of new enzymes.

Mutation of arginine 96 to lysine resulted in a reduction in activity for all substrates, but was more deleterious on the activity of dianionic substrates. The comparative mutagenesis

results of the two active site arginines in PP1 echoes the observation that lysine, rather than arginine, is found in the active sites of enzymes that hydrolyze monoanionic versus dianionic substrates. Except for enzymes that use a dinuclear metal center to bind the substrate, arginine is commonly found in active sites of phosphomonoesterases (PTPs, alkaline phosphatases, acid (histidine) phosphatases), while lysines are typically found in the active sites of enzymes that hydrolyze monoanionic phosphate diesters or sulfate esters.

### **Supporting Information**

Formulas used for calculation of kinetic isotope effects; conditions used for enzymatic activity assays using HPLC; sample Michaelis-Menten plot of kinetic and inhibition data; kinetic data for the reactions of substrates **1a – 5a** by native PP1 and mutants at pH 7.0.

The Supporting Information is available free of charge on the ACS Publications website.

### **Acknowledgment**

This work was supported by a grant from the National Institutes of Health to A.C.H. (GM47297) and by a grant from the Biology and Biotechnology Science Research Council to N.H.W. (C18734).

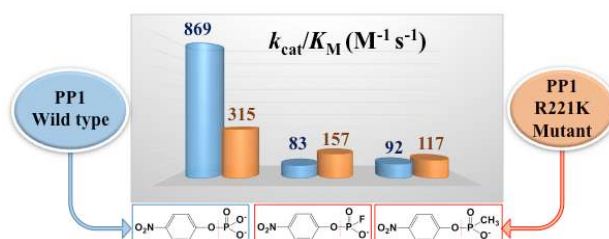
## References

- [1] Jensen, R. A. (1976) Enzyme Recruitment in Evolution of New Function, *Annu. Rev. Microbiol.* **30**, 409-425.
- [2] O'Brien, P. J., and Herschlag, D. (1999) Catalytic promiscuity and the evolution of new enzymatic activities, *Chemistry & Biology* **6**, R91-R105.
- [3] Jonas, S., and Hollfelder, F. (2009) Mapping catalytic promiscuity in the alkaline phosphatase superfamily, *Pure and Applied Chemistry* **81**, 731-742.
- [4] Bornscheuer, U. T., and Kazlauskas, R. J. (2004) Catalytic promiscuity in biocatalysis: using old enzymes to form new bonds and follow new pathways, *Angew. Chem. Int. Ed. Engl.* **43**, 6032-6040.
- [5] Crout, D. H. G., Dalton, H., Hutchinson, D. W., and Miyagoshi, M. (1991) Studies on Pyruvate Decarboxylase - Acyloin Formation from Aliphatic, Aromatic and Heterocyclic Aldehydes, *J. Chem. Soc. Perkin Trans. 1*, 1329-1334.
- [6] Kazlauskas, R. J. (2005) Enhancing catalytic promiscuity for biocatalysis, *Curr. Opin. Chem. Biol.* **9**, 195-201.
- [7] Roodveldt, C., and Tawfik, D. S. (2005) Shared promiscuous activities and evolutionary features in various members of the amidohydrolase superfamily, *Biochemistry* **44**, 12728-12736.
- [8] Gould, S. M., and Tawfik, D. S. (2005) Directed evolution of the promiscuous esterase activity of carbonic anhydrase II, *Biochemistry* **44**, 5444-5452.
- [9] Vick, J. E., Schmidt, D. M. Z., and Gerlt, J. A. (2005) Evolutionary potential of (beta/alpha)(8)-barrels: In vitro enhancement of a "new" reaction in the enolase superfamily, *Biochemistry* **44**, 11722-11729.
- [10] Aharoni, A., Gaidukov, L., Khersonsky, O., Gould, S. M., Roodveldt, C., and Tawfik, D. S. (2005) The 'evolvability' of promiscuous protein functions, *Nat. Genet.* **37**, 73-76.
- [11] Mohamed, M. F., and Hollfelder, F. (2013) Efficient, crosswise catalytic promiscuity among enzymes that catalyze phosphoryl transfer, *Biochim Biophys Acta* **1834**, 417-424.
- [12] Goldberg, J., Huang, H. B., Kwon, Y. G., Greengard, P., Nairn, A. C., and Kuriyan, J. (1995) Three-dimensional structure of the catalytic subunit of protein serine/threonine phosphatase-1, *Nature* **376**, 745-753.
- [13] McWhirter, C., Lund, E. A., Tanifum, E. A., Feng, G., Sheikh, Q. I., Hengge, A. C., and Williams, N. H. (2008) Mechanistic study of protein phosphatase-1 (PP1), a catalytically promiscuous enzyme, *J Am Chem Soc* **130**, 13673-13682.
- [14] Jencks, W. P., and Regenstein, J. (1976) Ionization Constants of Acids and Bases, In *Handbook of Biochemistry and Molecular Biology (Physical and Chemical Data)*, Third Edition. (Fasman, G. D., Ed.), p 314, CRC Press.
- [15] Bourne, N., and Williams, A. (1984) Effective Charge on Oxygen in Phosphoryl (-Po<sub>3</sub>-) Group Transfer from an Oxygen Donor, *J. Org. Chem.* **49**, 1200-1204.
- [16] Catrina, I. E., and Hengge, A. C. (1999) Comparisons of phosphorothioate and phosphate monoester transfer reactions: Activation parameters, solvent effects, and the effect of metal ions, *J. Am. Chem. Soc.* **121**, 2156-2163.
- [17] Holtz, K. M., Catrina, I. E., Hengge, A. C., and Kantrowitz, E. R. (2000) Mutation of Arg-166 of alkaline phosphatase alters the thio effect but not the transition state for phosphoryl transfer. Implications for the interpretation of thio effects in reactions of phosphatases, *Biochemistry* **39**, 9451-9458.
- [18] K. Hartke, and Bartulin, Q. F. J. (1962) Ringschlußreaktionen mit acylierten Carbodiimiden, *Angew. Chem.* **74**, 2.
- [19] Wittmann, R. (1963) Die Reaktion der Phosphorsäuren mit 2.4-Dinitro-fluorbenzol, I. Eine neue Synthese von Monofluorophosphorsäure-monoestern, *Chemische Berichte* **96**, 9.

- [20] Zalatan, J. G., and Herschlag, D. (2006) Alkaline phosphatase mono- and diesterase reactions: comparative transition state analysis, *J Am Chem Soc* 128, 1293-1303.
- [21] Ceulemans, H., and Bollen, M. (2004) Functional diversity of protein phosphatase-1, a cellular economizer and reset button, *Physiol. Rev.* 84, 1-39.
- [22] Zhang, A. J., Bai, G., Deans-Zirattu, S., Browner, M. F., and Lee, E. Y. (1992) Expression of the catalytic subunit of phosphorylase phosphatase (protein phosphatase-1) in *Escherichia coli*, *J. Biol. Chem.* 267, 1484-1490.
- [23] Zhang, Z. Y., Maclean, D., McNamara, D. J., Sawyer, T. K., and Dixon, J. E. (1994) Protein tyrosine phosphatase substrate specificity: size and phosphotyrosine positioning requirements in peptide substrates, *Biochemistry* 33, 2285-2290.
- [24] Kirby, A. J., and Varvoglis, A. G. (1967) The reactivity of phosphate esters. Monoester hydrolysis, *J. Am. Chem. Soc.* 89, 415-423.
- [25] Fasman, G. D. (1975) *Handb. Biochem. Mol. Biol.*
- [26] Baxter, N. J., Olguin, L. F., Golicnik, M., Feng, G., Hounslow, A. M., Bermel, W., Blackburn, G. M., Hollfelder, F., Waltho, J. P., and Williams, N. H. (2006) A Trojan horse transition state analogue generated by MgF<sub>3</sub>- formation in an enzyme active site, *Proceedings of the National Academy of Sciences of the United States of America* 103, 14732-14737.
- [27] Baxter, N. J., Blackburn, G. M., Marston, J. P., Hounslow, A. M., Cliff, M. J., Bermel, W., Williams, N. H., Hollfelder, F., Wemmer, D. E., and Waltho, J. P. (2008) Anionic charge is prioritized over geometry in aluminum and magnesium fluoride transition state analogs of phosphoryl transfer enzymes, *J Am Chem Soc* 130, 3952-3958.
- [28] Golicnik, M., Olguin, L. F., Feng, G. Q., Baxter, N. J., Waltho, J. P., Williams, N. H., and Hollfelder, F. (2009) Kinetic Analysis of beta-Phosphoglucomutase and Its Inhibition by Magnesium Fluoride, *J. Am. Chem. Soc.* 131, 1575-1588.
- [29] Hengge, A. C. (2002) Isotope effects in the study of phosphoryl and sulfuranyl transfer reactions, *Acc Chem Res* 35, 105-112.
- [30] Kirby, A. J., and Jencks, W. P. (1965) The reactivity of nucleophilic reagents toward the *p*-nitrophenyl phosphate dianion, *J. Am. Chem. Soc.* 87, 3209-3216.
- [31] E. J. Behrman, M. J. B., Herbert J. Brass, John Oelhaf. Edwards, Martin. Isaks. (1970) Reactions of phosphonic acid esters with nucleophiles. I. Hydrolysis, *J. Org. Chem.* 35, 7.
- [32] Kirby, A. J., Medeiros, M., Mora, J. R., Oliveira, P. S. M., Amer, A., Williams, N. H., and Nome, F. (2013) Intramolecular General Base Catalysis in the Hydrolysis of a Phosphate Diester. Computational Guidance to a Choice of Mechanism, *J. Org. Chem.* 78, 1343-1353.
- [33] van Loo, B., Jonas, S., Babbie, A. C., Benjdia, A., Berteau, O., Hyvonen, M., and Hollfelder, F. (2010) An efficient, multiply promiscuous hydrolase in the alkaline phosphatase superfamily, *Proc. Natl. Acad. Sci. U. S. A.* 107, 2740-2745.
- [34] Lassila, J. K., Zalatan, J. G., and Herschlag, D. (2011) Biological phosphoryl-transfer reactions: understanding mechanism and catalysis, *Annual review of biochemistry* 80, 669-702.
- [35] Hollfelder, F., and Herschlag, D. (1995) The nature of the transition state for enzyme-catalyzed phosphoryl transfer. Hydrolysis of O-aryl phosphorothioates by alkaline phosphatase, *Biochemistry* 34, 12255-12264.
- [36] Alkherraz, A., Kamerlin, S. C. L., Feng, G. Q., Sheikh, Q. I., Warshel, A., and Williams, N. H. (2010) Phosphate ester analogues as probes for understanding enzyme catalysed phosphoryl transfer, *Faraday Discussions* 145, 281-299.
- [37] Catrina, I. E., and Hengge, A. C. (2003) Comparisons of phosphorothioate with phosphate transfer reactions for a monoester, diester, and triester: isotope effect studies, *J Am Chem Soc* 125, 7546-7552.
- [38] Hengge, A. C., Edens, W. A., and Elsing, H. (1994) Transition-State Structures for Phosphoryl-Transfer Reactions of P-Nitrophenyl Phosphate, *J. Am. Chem. Soc.* 116, 5045-5049.
- [39] Hengge, A. C., and Onyido, I. (2005) Physical organic perspectives on phospho group transfer from phosphates and phosphinates, *Curr. Org. Chem.* 9, 61-74.

- [40] Thatcher, G. R. J., and Kluger, R. (1989) Mechanism and Catalysis of Nucleophilic-Substitution in Phosphate-Esters, *Adv. Phys. Org. Chem.* 25, 99-265.
- [41] Burgess, J., Blundell, N., Cullis, P. M., Hubbard, C. D., and Misra, R. (1988) Evidence for Free Monomeric Thiometaphosphate Anion in Aqueous-Solution, *J. Am. Chem. Soc.* 110, 7900-7901.
- [42] Catrina, I., O'Brien, P. J., Purcell, J., Nikolic-Hughes, I., Zalatan, J. G., Hengge, A. C., and Herschlag, D. (2007) Probing the origin of the compromised catalysis of *E. coli* alkaline phosphatase in its promiscuous sulfatase reaction, *J. Am. Chem. Soc.* 129, 5760-5765.
- [43] Zhang, J., Zhang, Z., Brew, K., and Lee, E. Y. (1996) Mutational analysis of the catalytic subunit of muscle protein phosphatase-1, *Biochemistry* 35, 6276-6282.
- [44] Pabis, A., Duarte, F., and Kamerlin, S. C. (2016) Promiscuity in the Enzymatic Catalysis of Phosphate and Sulfate Transfer, *Biochemistry* 55, 3061-3081.
- [45] Coleman, J. E. (1992) Structure and Mechanism of Alkaline-Phosphatase, *Annu. Rev. Biophys. Biomol. Struct.* 21, 441-483.
- [46] Sigel, R. K. O., Song, B., and Sigel, H. (1997) Stabilities and structures of metal ion complexes of adenosine 5'-O-thiomonophosphate (AMPS(2-)) in comparison with those of its parent nucleotide (AMP(2-)) in aqueous solution, *J. Am. Chem. Soc.* 119, 744-755.
- [47] Wang, S. L., Karbstein, K., Peracchi, A., Beigelman, L., and Herschlag, D. (1999) Identification of the hammerhead ribozyme metal ion binding site responsible for rescue of the deleterious effect of a cleavage site phosphorothioate, *Biochemistry* 38, 14363-14378.
- [48] Li, L. (2003) The biochemistry and physiology of metallic fluoride: action, mechanism, and implications, *Crit Rev Oral Biol Med* 14, 100-114.
- [49] Schlichting, I., and Reinstein, J. (1999) pH influences fluoride coordination number of the AlFx phosphoryl transfer transition state analog, *Nat Struct Biol* 6, 721-723.
- [50] Toyoshima, C., Nomura, H., and Tsuda, T. (2004) Lumenal gating mechanism revealed in calcium pump crystal structures with phosphate analogues, *Nature* 432, 361-368.
- [51] Pinkse, M. W., Merckx, M., and Averill, B. A. (1999) Fluoride inhibition of bovine spleen purple acid phosphatase: characterization of a ternary enzyme-phosphate-fluoride complex as a model for the active enzyme-substrate-hydroxide complex, *Biochemistry* 38, 9926-9936.
- [52] Schenk, G., Elliott, T. W., Leung, E., Carrington, L. E., Mitic, N., Gahan, L. R., and Guddat, L. W. (2008) Crystal structures of a purple acid phosphatase, representing different steps of this enzyme's catalytic cycle, *Bmc Structural Biology* 8.
- [53] Zalatan, J. G., Catrina, I., Mitchell, R., Grzyska, P. K., O'Brien P, J., Herschlag, D., and Hengge, A. C. (2007) Kinetic isotope effects for alkaline phosphatase reactions: implications for the role of active-site metal ions in catalysis, *J. Am. Chem. Soc.* 129, 9789-9798.
- [54] Nikolic-Hughes, I., Rees, D. C., and Herschlag, D. (2004) Do Electrostatic Interactions with Positively Charged Active Site Groups Tighten the Transition State for Enzymatic Phosphoryl Transfer?, *J Am Chem Soc* 126, 11814-11819.
- [55] Zhang, Y. L., Hollfelder, F., Gordon, S. J., Chen, L., Keng, Y. F., Wu, L., Herschlag, D., and Zhang, Z. Y. (1999) Impaired transition state complementarity in the hydrolysis of O-arylphosphorothioates by protein-tyrosine phosphatases, *Biochemistry* 38, 12111-12123.
- [56] Cassel, D., and Glaser, L. (1982) Resistance to phosphatase of thiophosphorylated epidermal growth factor receptor in A431 membranes, *Proc. Natl. Acad. Sci. U. S. A.* 79, 2231-2235.
- [57] Liang, C. X., and Allen, L. C. (1987) Sulfur Does Not Form Double-Bonds in Phosphorothioate Anions, *J. Am. Chem. Soc.* 109, 6449-6453.
- [58] Iyengar, R., Eckstein, F., and Frey, P. A. (1984) Phosphorus Oxygen Bond Order in Adenosine 5'-O-Phosphorothioate Dianion, *J. Am. Chem. Soc.* 106, 8309-8310.
- [59] Huang, H. B., Horiuchi, A., Goldberg, J., Greengard, P., and Nairn, A. C. (1997) Site-directed mutagenesis of amino acid residues of protein phosphatase 1 involved in catalysis and inhibitor binding, *Proc. Natl. Acad. Sci. U. S. A.* 94, 3530-3535.

- [60] Andrews, L. D., Zalatan, J. G., and Herschlag, D. (2014) Probing the origins of catalytic discrimination between phosphate and sulfate monoester hydrolysis: comparative analysis of alkaline phosphatase and protein tyrosine phosphatases, *Biochemistry* 53, 6811-6819.
- [61] Sunden, F., AlSadhan, I., Lyubimov, A. Y., Ressler, S., Wiersma-Koch, H., Borland, J., Brown, C. L., Jr., Johnson, T. A., Singh, Z., and Herschlag, D. (2016) Mechanistic and Evolutionary Insights from Comparative Enzymology of Phosphomonoesterases and Phosphodiesterases across the Alkaline Phosphatase Superfamily, *J. Am. Chem. Soc.* 138, 14273-14287.
- [62] Sunden, F., Peck, A., Salzman, J., Ressler, S., and Herschlag, D. (2015) Extensive site-directed mutagenesis reveals interconnected functional units in the alkaline phosphatase active site, *Elife* 4.
- [63] O'Brien, P. J., and Herschlag, D. (1998) Sulfatase activity of E-coli alkaline phosphatase demonstrates a functional link to arylsulfatases, an evolutionarily related enzyme family, *J. Am. Chem. Soc.* 120, 12369-12370.



TOC graphic